


ORIGINAL ARTICLE

F5-Atlanta: A novel mutation in F5 associated with enhanced East Texas splicing and FV-short production

Karen L. Zimowski¹  | Teodolinda Petrillo² | Michelle D. Ho² | Julie Wechsler¹ | Jordan E. Shields¹ | Gabriela Denning³ | Navdeep Jhita³ | Angel A. Rivera³ | Miguel A. Escobar⁴ | Christine L. Kempton⁵ | Rodney M. Camire^{2,6} | Christopher B. Doering¹

¹Aflac Cancer and Blood Disorders Center, Emory University/Children's Healthcare of Atlanta, Atlanta, Georgia, USA

²The Children's Hospital of Philadelphia, The Raymond G. Perelman Center for Cellular and Molecular Therapeutics, Philadelphia, Pennsylvania, USA

³Expression Therapeutics, Tucker, Georgia, USA

⁴University of Texas Houston Health Science Center, Houston, Texas, USA

⁵Department of Hematology and Medical Oncology, Emory University School of Medicine, Atlanta, Georgia, USA

⁶Division of Hematology, Department of Pediatrics, Perelman School of Medicine, The University of Pennsylvania, Philadelphia, Pennsylvania, USA

Correspondence

Christopher B. Doering, Emory Children's Center, Room 450, 2015 Uppergate Drive, Atlanta, GA 30322, USA.
Email: cdoerin@emory.edu

Funding information

National Institutes of Health/National Heart, Lung and Blood Institute, Grant/Award Number: R56-HL131059, R01-137128, R01-HL131833 and P01-HL139420; NHF-Shire Clinical Fellowship Program; Pfizer Global ASPIRE Gene and anti-TFPI Therapies Hemophilia Program, Grant/Award Number: WI242430

Abstract

Background: Elucidating the molecular pathogenesis underlying East Texas bleeding disorder (ET) led to the discovery of alternatively spliced *F5* transcripts harboring large deletions within exon 13. These alternatively spliced transcripts produce a shortened form of coagulation factor V (FV) in which a large portion of its B-domain is deleted. These FV isoforms bind tissue factor pathway inhibitor alpha (TFPI α) with high affinity, prolonging its circulatory half-life and enhancing its anticoagulant effects. While two missense pathogenic variants highlighted this alternative splicing event, similar internally deleted FV proteins are found in healthy controls.

Objective: We identified a novel heterozygous 832 base pair deletion within *F5* exon 13, termed *F5-Atlanta* (*F5-ATL*), in a patient with severe bleeding. Our objective is to investigate the effect of this deletion on *F5* and FV expression.

Methods & Results: Assessment of patient plasma revealed markedly elevated levels of total and free TFPI and a FV isoform similar in size to the FV-short described in ET. Sequencing analyses of cDNA revealed the presence of a transcript alternatively spliced using the ET splice sites, thereby removing the *F5-ATL* deletion. This alternative splicing pattern was recapitulated by heterologous expression in mammalian cells.

Conclusions: These findings support a mechanistic model consisting of cis-acting regulatory sequences encoded within *F5* exon 13 that control alternative splicing at the ET splice sites and thereby regulate circulating FV-short and TFPI α levels.

KEYWORDS

alternative splicing, blood coagulation disorder, factor V, hemostasis, transcriptome

Presented in abstract form at the 59th annual meeting of the American Society of Hematology, Atlanta, GA, December 10, 2017.

Manuscript handled by: Alan Mast

Final decision: Alan Mast, 22 March 2021

© 2021 International Society on Thrombosis and Haemostasis

1 | INTRODUCTION

Coagulation factor V (FV) plays a pivotal role in hemostasis. As part of the prothrombinase complex, activated FV (FVa) serves as a cofactor for activated factor X (FXa) on a negatively charged phospholipid surface and accelerates the conversion of prothrombin to thrombin. FV is a 330-kDa protein organized into an A1-A2-B-A3-C1-C2 domain structure homologous to factor VIII (FVIII). In human FV, the heavily glycosylated B-domain represents ~50% of the protein's mass and is encoded entirely by exon 13.¹⁻⁴ FV circulates in plasma as a procofactor and lacks procoagulant function until proteolytic processing at Arg-709, Arg-1018, and Arg-1545 removes the B-domain and generates FVa.^{5,6} Our group has uncovered the importance of two regions within the B-domain, a basic region (BR; amino acids 963-1008) and acidic region 2 (AR2; amino acids 1493-1537), whose interaction is necessary for maintaining an inactive procofactor state.⁷⁻¹⁰ Disruption of this interaction through deletion of the BR yields a protein with cofactor-like properties and addition of the BR fragment *in trans* blocks FV procoagulant activity.⁸

Genetic alterations in the FV gene (*F5*) typically result in FV deficiency and produce a mild clinical bleeding phenotype. However, two variants within exon 13, c.2350A>G (originally reported as c.A2440G, East Texas bleeding disorder, ET) and c.2588C>G (FV-Amsterdam), result in moderate bleeding diatheses that are not associated with decreased FV activity but promote bleeding presumably through stabilizing the anticoagulant protein, tissue factor pathway inhibitor (TFPI).¹¹⁻¹³ TFPI is a Kunitz-type serine protease inhibitor that both directly inhibits FXa and blocks the extrinsic coagulation pathway through the formation of TFPI-FXa-tissue factor (TF)-activated factor VII (FVIIa) quaternary complex.¹⁴⁻¹⁷ There are two major isoforms of TFPI, TFPI α and TFPI β . TFPI α is the only isoform that can associate with certain forms of FV.¹⁸⁻²⁰ It consists of three Kunitz-type domains (K1, K2, and K3) and a basic C-terminus, which is homologous to the FV BR. The K1 and K2 domains bind and inhibit the active sites of FVIIa and FXa,²¹ respectively, while the K3 domain binds protein S, localizing TFPI α to membrane surfaces.^{22,23} A functional link between FV and TFPI α was originally described by Mast and Broze.²⁴ Patients with FV deficiency have reduced levels of TFPI α , suggesting these proteins interact in plasma.^{25,26}

In ET, an apparently missense mutation in *F5* exon 13 promotes alternative splicing through enhancement of a cryptic splice site. Splicing at the ET splice sites removes 2106 bp from exon 13 and produces an internally deleted FV protein, termed FV-short. FV-short contains a B-domain missing the functionally important BR but retaining an exposed AR2. As such, FV-short is constitutively active and should promote thrombin generation. However, through the exposed AR2, FV-short binds the basic C-terminus of TFPI α with high affinity resulting in increased circulating TFPI α levels. While FV-short is found at low (subnanomolar) levels in normal plasma, it is increased 10-fold in ET.¹³ High levels of TFPI α in ET coupled with the alteration in FV-short function are thought to contribute to the bleeding diathesis in these patients.^{27,28} The functional impact of this interaction has relevance beyond ET. In collaborative studies, we have shown that TFPI α , via its C-terminal tail,

Essentials

- Alternative splicing of *F5* exon 13 creates factor V (FV)-short, an isoform that binds and stabilizes tissue factor pathway inhibitor alpha (TFPI α).
- *F5-Atlanta* (*F5-ATL*) is a novel *F5* exon 13 deletion identified in a patient with severe bleeding.
- *F5-ATL* enhances *F5* alternative splicing, markedly increasing FV-short levels.
- *F5-ATL* suggests regulatory sequences in *F5* exon 13 that govern FV-short and TFPI levels.

binds naturally occurring plasma FV activation intermediates and platelet FV that retain an exposed AR2 and prevents the ability of the cofactor to assemble in prothrombinase.²⁰ Thus, TFPI α not only regulates FXa-TF-FVIIa but may play an important role in regulating coagulation initiation at the level of prothrombinase.^{20,29,30} The degree to which TFPI α impacts prothrombinase assembly is likely related to the levels of FV species that can engage TFPI α , including partially cleaved FV, platelet-derived FV, and FV-short. Herein, we identify and characterize a novel deletion in *F5* exon 13, termed *F5-Atlanta* (*F5-ATL*). Compared to ET and FV-Amsterdam, *F5-ATL* results in significantly higher plasma levels of both FV-short and TFPI α through a previously undescribed mechanism that suggests the importance of this region in modulating ET splicing, FV-short production, and circulating TFPI α levels.

2 | MATERIALS AND METHODS

2.1 | Clinical data and processing of human samples

Human subject research was completed according to institutional review board-approved protocols and per the Declaration of Helsinki. Clinical data was obtained through review of the patient's medical record. Whole blood from the patient and a healthy volunteer was collected into 3.2% buffered sodium citrate. The samples were centrifuged at 1260 g for 15 min. Plasma was removed into a cryogenic vial and the remainder of the whole blood was frozen at -80°C. The plasma was centrifuged again at 1260 g for 15 min and aliquoted prior to freezing at -80°C.

2.2 | Thrombin generation assay

Thrombin generation assay (TGA) was performed on plasma from the *F5-ATL* patient, an affected patient from the initial ET cohort (patient IV:9),¹² and pooled normal human plasma (NHP) (George King Bio-Medical) before and after addition of a mixture of monoclonal antibodies targeting the K1, K2, K3, and C-terminal domain of TFPI (25 μ g/ml each; Cell Sciences). TGA was triggered by 0.4 pM tissue

factor (Dade® Innovin®, Siemens Healthcare), relipidated into 75:25 phosphatidylcholine and phosphatidylserine (4 μ M final; Avanti Polar Lipids Inc.) followed by the cleavage of the fluorogenic substrate Z-Gly-Gly-Arg-AMC HCl (Bachem) as previously described.^{31,32}

2.3 | Determining plasma concentrations of TFPI, FV, and FV-short

TFPI (total and free), FV, and FV-short levels in patient plasma were determined and compared to the concentration measured in NHP, FV-deficient plasma (FV-DP; George King Biomedical), and plasma from ET (F5-ET). The TFPI concentration was determined using ELISA kits (Asserachrom Total and Free TFPI, Diagnostica Stago Inc.) following the manufacturer's recommendation and are the average of at least three technical replicates. FV and FV-short levels were estimated using western blotting. Standard curves for FV (2–15 nM) and FV-short (10–80 nM) were obtained by diluting NHP (FV concentration of 20 nM) or recombinant FV-short (expressed as previously described⁷) in FV-DP. Samples containing 2 μ l of plasma were subjected to sodium dodecyl sulfate polyacrylamide gel electrophoresis (3%–8% gradient) under reducing conditions and blotted onto nitrocellulose membranes. FV and FV-short were visualized with murine monoclonal antibodies against FV heavy chain (AHV-5146, Haematologic Technologies Inc.) labelled with infrared dye IRDye680 (LiCor). Blots were scanned using an infrared laser (Odyssey, LI-COR), and signal intensities were assessed using the Image Studio Lite software (LI-COR).

2.4 | Sequencing analyses

Genomic DNA was isolated from peripheral blood using the QiaAmp DNA Blood kit. *F5* exon 13 was polymerase chain reaction (PCR)-amplified, gel purified, and Sanger sequencing was performed. Sequencing primers are available in Table S3 in supporting information. Commercial sequencing (Prevention Genetics) using DNA next-generation sequencing was completed to assess potential confounding variations. For mRNA analysis, total RNA was isolated using RNeasy Blood kit, including an on-column DNase digestion. cDNA was generated (Invitrogen's Superscript III reverse transcriptase with OligoDTs), and Sanger sequencing was performed. For RNAseq, total RNA samples were assessed for RNA integrity using an Agilent 2100 bioanalyzer, and samples passing quality control standards (RIN > 6.8 and OD_{260/280} > 2) were used for library preparation via Illumina Platform PE150 (Novogene) at a read depth of 100 million reads per sample after excluding globin. Raw sequence reads were tested for quality control,³³ and Illumina adapter sequences were removed. Cleaned reads were aligned to the hg38 human genome (UCSC) using STAR aligner 2.5.2 in two-pass mode.³⁴ Parameters used are available upon request. Resulting .bam files were indexed and processed using Samtools 1.3³⁵ and Picard Tools 2.6.0,³⁶ where duplicates were marked but not removed, and reads were selected

that corresponded to *F5* exon 13 (chr1:169,539,056–169,544,275). Data were visualized using the Integrative Genomics Viewer 2.8.0.³⁷

2.5 | Construction of *F5* variants

Human *F5* cDNA within a pED plasmid was used as a template for creating mutant expression vectors. The *F5* cDNA sequence contained the polymorphisms associated with the G-allele (c.2301A>G, c.2776A>G, c.2573A>G, and c.2594A>G).³⁸ Gene fragments containing the ET point mutation (gBlocks, Integrated DNA Technologies) and the *F5*-ATL cDNA sequence (GenScript) were synthesized and subcloned into pED and pCDNA5/FRT/TO expression vectors.

2.6 | DNA transfection and analysis of conditioned media

Recombinant wild-type (wt) and mutant pED *F5* vectors were linearized and co-transfected into baby hamster kidney (BHK) cells with a linearized gene fragment containing puromycin resistance (from pLKO.1 puro plasmid) at a 50:1 molar ratio to create stably transfected colonies. FLP-INTM 293 human embryonic kidney (HEK) cells (Invitrogen) were utilized with the pCDNA5/FRT/TO plasmid to create stably transfected cells. All transfections were completed with Lipofectamine 2000 (Invitrogen). Clones were screened for FV activity using a one-stage FV clotting assay.

2.7 | Reverse transcription and real-time PCR

Total RNA was isolated from mammalian cells using RNeasy with on-column DNase digestion (Qiagen), and reverse transcription was performed using SuperScript VILO Reverse Transcriptase (Invitrogen). Exon 13 splice variants were amplified using Hot Start Taq 2X Master Mix (New England BioLabs). The PCR was initiated at 95°C for 30 s, amplified with 30 cycles of 30 s at 95°C, 60 s at 54–58°C, and 75–90 s at 68°C, with a final elongation of 5 min at 68°C. PCR primers are detailed in Table S4 in supporting information.

3 | RESULTS

3.1 | Clinical features

A 43-year-old African American male with a history of prolonged bleeding since infancy including circumcision-induced and umbilical stump bleeding, excessive trauma-associated bleeding, and recurrent spontaneous intramuscular hematomas was referred to hematology for evaluation of abnormal bleeding. His family history is notable for a father who died from a trauma-induced injury. Laboratory evaluation (Table 1) revealed prolonged prothrombin time (PT) and activated partial thromboplastin time (APTT) that failed to correct after

TABLE 1 Clinical laboratory evaluation assessing etiology of bleeding tendency

Laboratory test	F5-ATL patient	Normal range
PT (s)	25.9	9.4–12.5
PT mixing study (s)	15.9	11.2
APTT (s)	58.8	25–36.5
APTT mixing study (s)	Immediate: 50.2 Incubated: 49.8	Immediate: 34.3 Incubated: 34.8
Fibrinogen, mg/dl	352	200–393
Factor II (IU/dl)	77	79–131
Factor V (IU/dl)	125	62–139
Factor VII (IU/dl)	72	63–174
Factor VIII (IU/dl)	170	50–185
Factor IX (IU/dl)	90	65–150
Factor X (IU/dl)	72	50–185
Factor XI (IU/dl)	69	65–150
Factor XIII (IU/dl)	128	67–173
Thrombin time (s)	11.6	<16.6
α 2-antiplasmin (IU/dl)	128	82–133
Plasminogen activator inhibitor-1, IU/ml	26.1	<37
Euglobulin lysis time (min)	>120	>120
VWF antigen (IU/dl)	153	53–270
VWF ristocetin cofactor (IU/dl)	142	50–180

Abbreviations: APTT, activated partial thromboplastin time; IU/dL, international units per deciliter; min, minutes; PT, prothrombin time; sec, seconds; VWF, von Willebrand factor.

50:50 mixing with NHP, and normal factor activity levels.³⁹ A lupus anticoagulant was not detected. His platelet count and platelet aggregation studies were normal.

3.2 | Elevated TFPI and FV-short result in impaired initiation of coagulation

As the clinical findings and laboratory data were inconclusive, further diagnostics were performed. TGA revealed a prolonged lag time (14 min) compared to a normal control (5 min) and plasma from the original ET family (10.5 min). Unexpectedly, the peak thrombin was similar between NHP and ET plasma. This finding is likely attributable to differences in pre-analytical processing, inconsistencies amongst NHP, and lack of standardization and variability in the TGA.^{40–42} The addition of a cocktail of anti-TFPI antibodies in both patient and ET plasma corrected the delayed lag time and resulted in robust peak thrombin generation higher than seen in equivalently blocked NHP (Figure 1A, Table S1 in supporting information). Further, the addition of the anti-TFPI antibody mixture corrected the prolonged PT in both patient and ET plasma (data not shown). The patient's total TFPI

(24.0 ± 2.8 nM) and free TFPI (6.9 ± 2.0 nM) levels were 11- and 22-fold higher compared to NHP, respectively. Furthermore, these levels were greater than observed in ET patient plasma, in which total TFPI and free TFPI were 4- and 5-fold higher than NHP, respectively (Figure 1B, Table S2 in supporting information).

As TFPI α has been shown to form a complex with FV-short,¹³ patient plasma was analyzed for the presence of this FV isoform. Western blot analysis using an anti-FV heavy chain antibody revealed the presence of full-length (FL)-FV (330 kDa) as well as a smaller isoform, presumably representing FV-short, as it was identical in size to that seen in ET plasma (250 kDa) and to purified recombinant FV-short added to plasma (Figure 1C). As there are no available assays to quantify plasma FV-short, recombinant FV-short was used to generate a standard curve, and western blotting was used to compare NHP, F5-ATL patient plasma, and ET patient plasma. These analyses demonstrated higher levels of FV-short (45 nM) in F5-ATL patient plasma compared to plasma from ET (7 nM) and NHP (<0.5 nM; Figure 1D, Table S2). Therefore, the robust thrombin generation seen following TFPI blockade likely is attributable to extremely elevated levels of FV-short being outcompeted from TFPI α in the presence of anti-TFPI antibody treatment.

3.3 | Identification of a large deletion in exon 13 of F5 and evidence of alternative splicing

Because the clinical and biochemical findings were consistent with an ET-like disorder, PCR-based analysis on both genomic DNA and cDNA focusing on F5 exon 13 was performed along with Sanger sequencing. For reference, Figure 2A depicts F5 exons 12–14, the surrounding intron and ET-splicing boundaries, and all PCR primer locations. Amplification of the complete exon 13 from genomic DNA revealed both the expected 3476 base pair (bp) fragment and a smaller 2644 bp amplicon that was unique to the patient sample (Figure 2B, red arrows). Sanger sequencing of the PCR products revealed that while the larger amplicon represented the expected F5 exon 13 sequence, the smaller product contained a large internal exon 13 deletion. Commercial next-generation sequencing of patient genomic DNA confirmed an 832 bp deletion in F5 exon 13 (F5: c.2413_3244del [p. Thr805Serfs*13]), located 3' to the 5' ET splice site, which we designated "F5-Atlanta" (F5-ATL; Table S5 in supporting information). This deletion predicts the omission of 277 amino acids, a frameshift, translation of 12 non-native amino acids, and insertion of a premature termination codon. Next-generation sequencing also identified two variants of uncertain significance in F8 and F11 that are predicted to be benign. The F8 missense variant (c.4333 T>C, p. Ser1445Pro) has been previously reported in two patients with hemophilia⁴³; however, the patient's FVIII activity (170 IU/dl) suggests this variant does not contribute to his bleeding. The F11 missense variant (c.197C>T, p. Pro66Leu, rs5968) has not been previously reported; however, partial factor XI deficiency alone would not account for the patient's severe bleeding. In addition, several predicted non-pathogenic single nucleotide polymorphisms were identified in F5 exon 13.³⁸

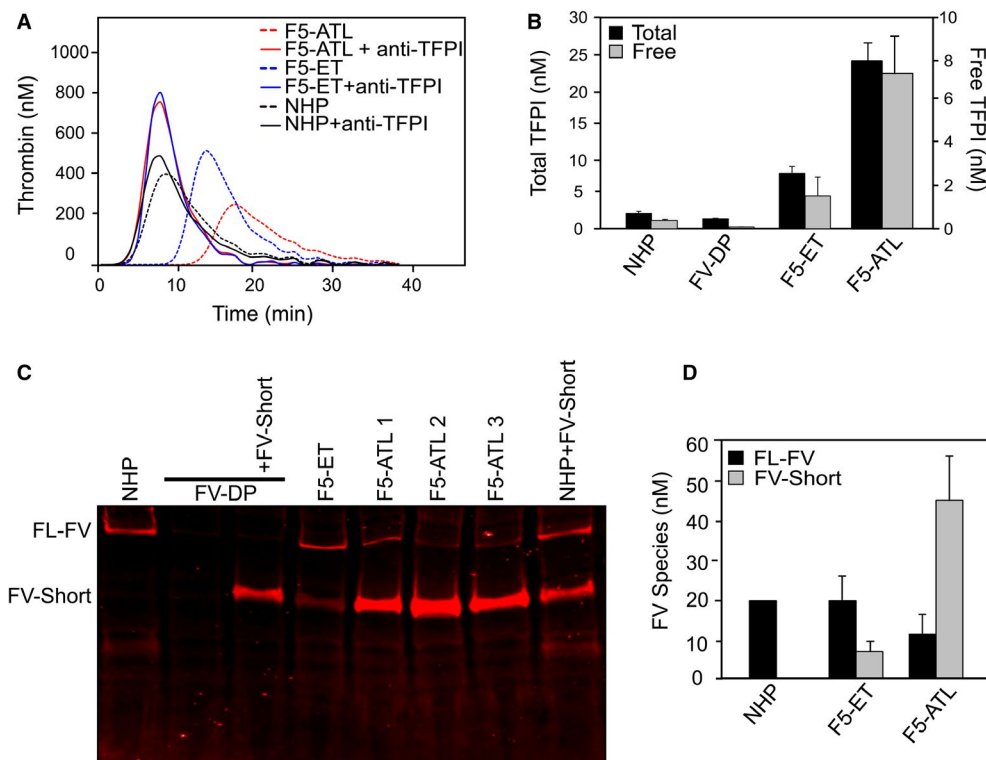


FIGURE 1 Thrombin generation and plasma tissue factor pathway inhibitor (TFPI) and factor V (FV)-short levels in the affected patient. (A) Thrombin generation was measured in normal human plasma (NHP) and patient citrated plasma (F5-ATL) in the presence or absence of 100 μ g/ml anti-TFPI antibodies directed against all domains. (B) ELISA for TFPI: TFPI (total and free) in patient plasma was measured and compared to the concentration in NHP, FV-deficient plasma (FV-DP), and East Texas bleeding disorder (ET) patient plasma (F5-ET). The TFPI concentrations reported are mean \pm sample standard deviation of at least three technical replicates. (C) Immunoblotting of 2 μ l of patient plasma (F5-ATL) compared to F5-ET, NHP, and FV-DP with and without 20 nM recombinant FV-short. FV was detected using an anti-FV heavy chain monoclonal antibody directly labeled with IRDye680. Representative patient samples collected over three visits from May 2016 to August 2017 were used and (D) mean (\pm sample standard deviation) concentrations of full-length (FL)-FV and FV-short levels in patient plasma in comparison to those seen with F5-ET and NHP were determined. nM, nanomolar; min, minutes

Based on the presence of a premature stop codon, *F5-ATL* should result in a functionally null allele and therefore decreased plasma FV activity. However, the patient's FV activity was 125%. To reconcile this difference, real-time (RT)-PCR and sequencing analysis was performed. Using primers located in *F5* exons 12 and 14 (Figure 2C, blue arrows), RT-PCR demonstrated three amplicons: a 3169 bp amplicon, which was predominantly seen in the control and aligned with *F5* on sequencing; an intermediate-sized amplicon (1063 bp), which was most evident in the patient sample; and a small minor transcript (384 bp) visualized in the control sample. Sanger sequencing of the 1063 bp amplicon confirmed the in-frame removal of 2106 bp flanked by the ET splice donor/acceptor sites. Sequencing of the smallest amplicon revealed exon 13 skipping. Surprisingly, no transcript corresponding to *FL-F5* was detected in the patient sample. This was unexpected as *F5-ATL* is a heterozygous deletion, and the patient's plasma FL-FV concentration was approximately one-half that seen in NHP (Figure 1D, Table S2). We speculate that the lack of a *FL-F5* amplicon in *F5-ATL* results from enhanced PCR kinetics for the shorter ET-spliced product. To confirm the presence of a *FL-F5* transcript in the *F5-ATL* sample, RT-PCR was completed using primers directly flanking

F5-ATL with the reverse primer located in the region removed during ET-splicing and revealed a prominent band representing *FL-F5* (Figure 2D, black arrows).

To further visualize the degree to which *F5-ATL* is associated with ET-splicing, RT-PCR analysis was completed using primers directly flanking the ET splice sites (Figure 2E, green arrows). A shortened PCR extension time was utilized in this experiment to enhance visualization of *F5-short* transcripts. Again, only an ET-spliced *F5* transcript was visualized using patient cDNA with no corresponding *FL-F5* transcript, a finding also attributed to PCR kinetics. The control samples revealed a large amplicon consistent with *FL-F5* and a 189 bp amplicon corresponding to the expected size for ET-spliced *F5-short*. An additional alternatively spliced *F5* cDNA transcript was identified in control human liver which on Sanger sequencing revealed a previously undescribed transcript utilizing cryptic non-consensus splice sites. Although the RT-PCR results clearly demonstrate increased *F5-short* transcripts in patient samples, the sequence complexity of *F5* exon 13, including its highly repetitive nature, as well as the presence of this unexpected alternatively spliced transcript similar to *F5-short*, precluded further quantitative assessment of transcript abundance using PCR-based methods.

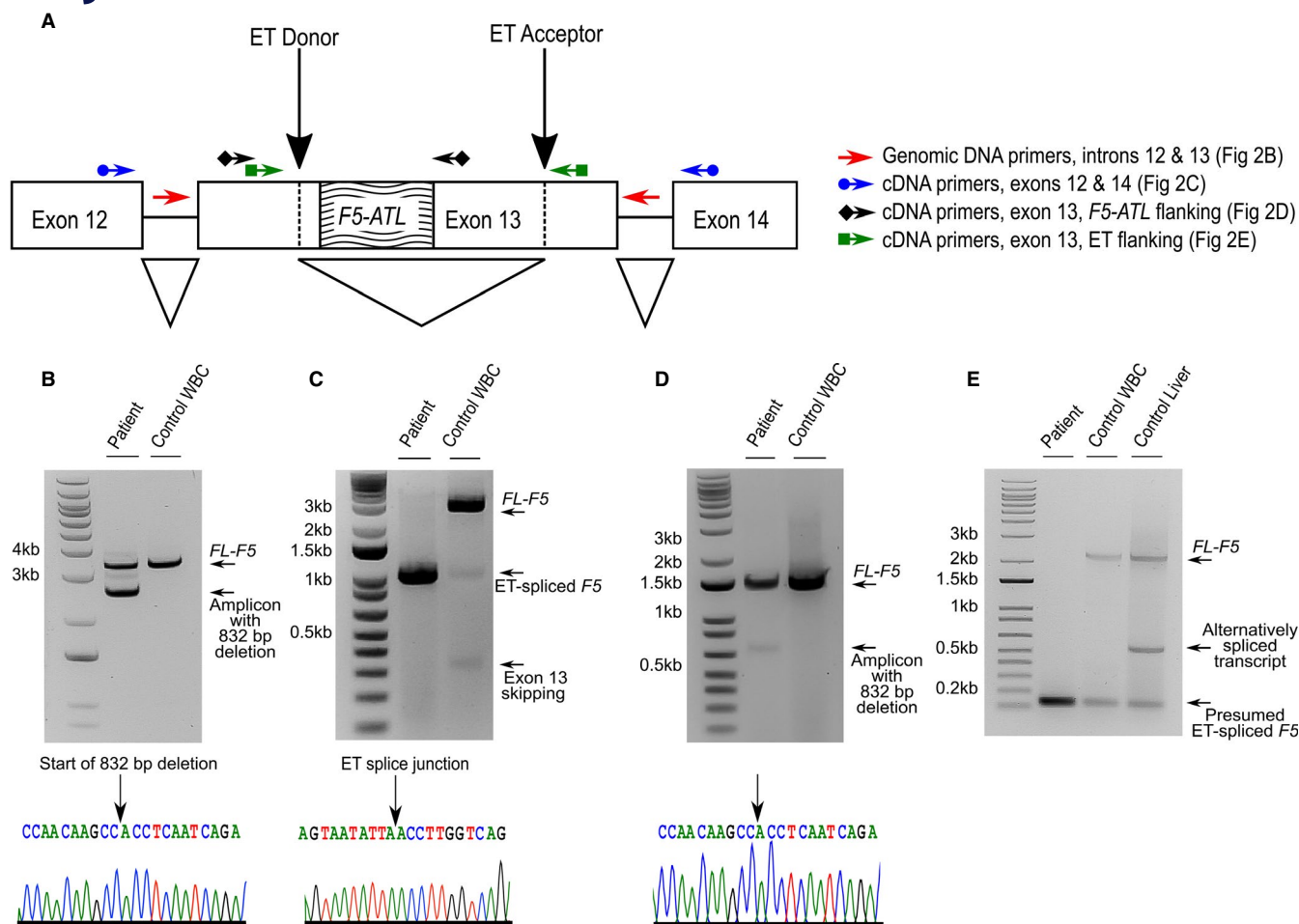


FIGURE 2 Genetic analysis of patient *F5* reveals a large deletion and enhanced East Texas bleeding disorder (ET) splicing. (A) Schematic of *F5* exons 12–14, the surrounding intron and ET-splicing boundaries, and all polymerase chain reaction (PCR) primer locations. Diagram of *F5* is not drawn to scale. Adapted from Vincent et al.¹³ (B) PCR amplification of genomic DNA (genomic primers, red arrows) followed by Sanger sequencing of the smallest amplicon in the patient sample revealed a large internal deletion starting at the central ACC sequence in the chromatogram (arrow). (C) Real-time (RT)-PCR using primers located in exons 12 and 14 (cDNA primers, blue arrows) demonstrated a FL-*F5* transcript (3169 bp amplicon) in the control sample and a smaller transcript (1063 bp amplicon) in the patient sample. Sanger sequencing of the 1063 bp amplicon confirmed the in-frame removal of 2106 bp flanked by the ET splice sites (ET splice junction on chromatogram: arrow). (D) RT-PCR using primers flanking the *F5*-ATL deletion (cDNA primers, black arrows) confirmed the presence of FL-*F5* in the patient sample; Sanger sequencing of the faint amplicon revealed the 832 bp deletion. (E) RT-PCR using primers flanking the ET splice sites (cDNA primers, green arrows) demonstrated a FL-*F5* transcript and a transcript of 189 bp corresponding to the expected size for ET-spliced *F5*-short. An additional alternatively-spliced *F5* cDNA transcript was identified in human total liver RNA. bp, base pairs; kb, kilobase pairs; WBC, white blood cells

RNAseq represents a high-resolution tool for the characterization of mRNA isoforms and has not been reported for *F5*-short analysis. Using patient leukocytes, control leukocytes, and control liver total RNA samples, RNAseq was performed to further examine the impact of *F5*-ATL on *F5* and *F5*-short mRNA production. Using the Sashimi plot tool from the Integrative Genomics Viewer, splice junction analysis of the aligned reads spanning *F5* exon 13 revealed the expected splicing at intron junctions. However, a large splicing junction or deletion in the middle of exon 13 was detected in the patient samples (Figure 3A, bottom). This event was observed in an average of 103 reads (Table 2). The boundaries of this junction corresponded precisely with the ET splice sites (splice junction coordinates: chr1:169540633–169542739). On average 233 reads in

the patient samples showed constitutive intron 12 splicing. Based on this, ET splicing was present in 44% of the contiguous sequences generated from the patient samples. Using two polymorphisms, allele mapping determined that the ET-spliced sequences originated from the *F5*-ATL allele. Additionally, all *F5* exon 13 polymorphisms identified on next-generation sequencing were located on the non-deletional allele. No large junctions with boundaries corresponding to an 832 bp deletion were identified in the patient, and no large deletions or splicing junctions, including ET-splicing, were identified in control samples (Figure 3A, top). The lack of ET-spliced transcripts in control samples is likely related to the low abundance of *F5*-short (<0.5 nM) in healthy individuals and the decreased sensitivity of short-read RNAseq for detecting low-abundance transcripts.^{44,45}

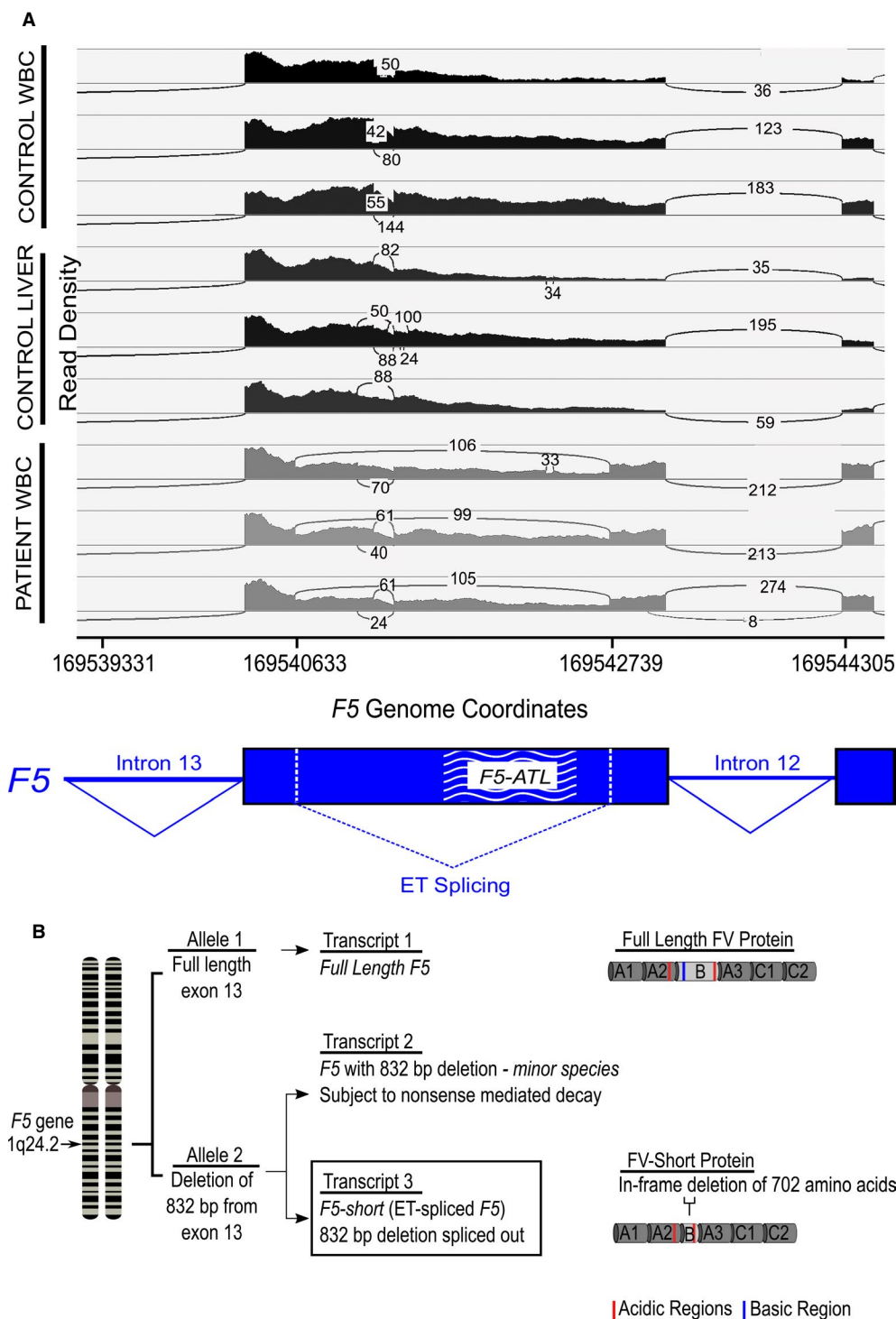


FIGURE 3 RNAseq reveals an altered *F5* transcriptome derived from the patient's variant allele. (A) Sashimi plot showing RNAseq coverage and splice junctions across *F5* exon 12 through intron 13 from control WBC, control liver, and patient WBC. The y-axis of each histogram represents the read density, and the x-axis shows the *F5* genome coordinates. The curved lines demarcate deletion or splicing junctions with the number of reads spanning each junction denoted within each corresponding arc. A large (2106 bp) deletion/splicing junction was visualized within exon 13 of the patient samples (bottom three histograms) with the junction boundaries mapping precisely to the genome coordinates of the East Texas (ET) splice sites. Three technical replicates were done for each sample. (B) Summary of findings from the patient's *F5* sequencing analyses. WBC, white blood cells; bp, base pairs

Several common small deletions or splice junction sites were identified in both the control and patient samples; the significance of these remains unclear. Collectively, the RNAseq data suggest the

F5-ATL allele is transcribed at levels similar to the non-*F5-ATL* allele, and *F5-ATL* containing pre-mRNA are efficiently spliced using the ET splice sites. These findings further suggest that ET splicing

Sample	Reads spanning F5 Exon 13	Reads with a large deletion/splice junction	Reads with a common small deletion/splice junction
Control WBC 1	1024	0	50
Control WBC 2	2915	0	122
Control WBC 3	4286	0	19
Control liver 1	2878	0	116
Control liver 2	5387	0	253
Control liver 3	3578	0	88
Patient WBC 1	2185	106	103
Patient WBC 2	2481	99	101
Patient WBC 3	2614	105	85

TABLE 2 Absolute read counts from RNAseq comparing the number of shared large and small deletion/splice junctions

Abbreviation: WBC, white blood cell.

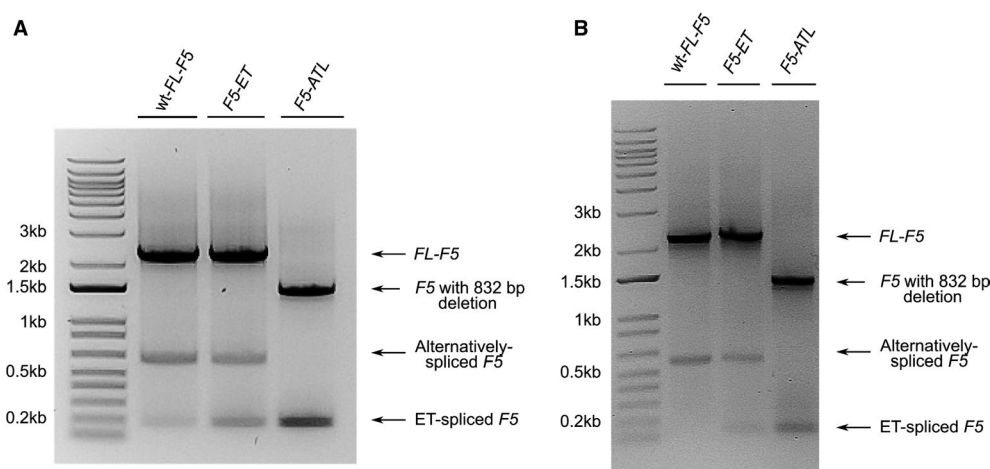


FIGURE 4 *F5-ATL* induces alternative splicing *in vitro*. Plasmids containing human wild-type full-length *F5* cDNA (wt-FL-*F5*), *F5* cDNA with the East Texas bleeding disorder (ET) point mutation (*F5-ET*), and *F5* cDNA with the *F5-ATL* deletion (*F5-ATL*) were transfected into mammalian cells, and total RNA was isolated. (A) Real-time polymerase chain reaction (RT-PCR) was utilized to qualitatively assess differential splicing of the primary *F5* transcripts among the variant BHK cell lines. (B) RT-PCR was utilized to qualitatively assess differential splicing of the primary *F5* transcripts amongst the variant FLP-IN 293 HEK cell lines. Representative gels depict the results obtained from three independent experiments. RT-PCR primers flanked the ET splice sites and were located similar to those used in Figure 2E (cDNA primers, green arrows). FL, full-length; ET, East Texas bleeding disorder; BHK, baby hamster kidney; HEK, human embryonic kidney; bp, base pairs; kb, kilobase pairs

represents a rare event under normal conditions, which is consistent with the low FV-short plasma levels in healthy individuals. A summary of the *F5-ATL* genetic findings as well as the predicted *F5* transcripts and FV products are detailed in Figure 3B. As depicted, from the wt *F5* allele ("Allele 1"), a canonically spliced transcript is produced and yields a FL-FV protein. From the allele containing *F5-ATL* ("Allele 2"), two transcripts are possible. Canonical splicing of this allele creates a transcript containing a terminal frameshift that is subject to nonsense-mediated decay and therefore does not produce FV protein. The predominant transcript produced from the *F5-ATL* allele results from alternative splicing at the ET splice sites. Based on the location of the 832 bp deletion, this deletion is removed via ET splicing, and translation of the mature mRNA produces FV-short protein. Collectively, these results suggest that *F5-ATL* induces alternative splicing of *F5* exon 13 using the ET splice sites.

3.4 | Cell culture modeling of *F5-Atlanta*

As no other affected family members were identified to corroborate the findings seen in patient samples, we sought to examine the effect of *F5-ATL* on *F5* exon 13 splicing using a cell culture platform incorporating cDNAs containing expression plasmids for wt-FL-*F5*, *F5-ATL*, and *F5-ET* (i.e., wt-FL-*F5* with c.2350A>G) transfected into BHK and FLP-INTM-293 HEK cells. RT-PCR of total RNA using primers flanking the ET splice sites (similar to Figure 2A, green arrows) demonstrated the three expected products corresponding to FL-*F5*, FL-*F5* containing an 832 bp deletion, and ET-spliced *F5*. Note that in this model, the FL-*F5* product containing the 832 bp deletion was the predominant amplicon identified in the *F5-ATL* variants. In BHK cells, a faint band corresponding to ET-spliced *F5* was observed in the wt-FL-*F5* variant. Increasing intensity of the

		ET Donor Splice Site	ET Acceptor Splice Site
Primates	Human	AAGTAATATT AGTAAGT TCACTGT	CTTTTCCTTATCC CAGAC CTTG
	Colobus	AAATAATACT AGTAAG CTCACTGT	CTTTTCCTTATCC CAGAC CTTG
	Baboon	AAATAATATT AGTAGG CTCACTGT	CTTTTCCTTATCC CAGAC CTTG
	Rhesus Monkey	AAATAATATT AGTAAG CTCACTGT	CTTTTCCTTATCC CAGAC CTTG
	Macaque	AAATAATATT AGTAAG CTCACTGT	CTTTTCCTTATCC CAGAC CTTG
	Gibbon	AAGTAATATT AGTAAG CTCACTGT	CTTTTCCTTATCC CAGAC CTTG
	Orangutan	AAGTAATATT AGTAAG CTCACTGT	CTTTTCCTTATCC CAGAC CTTG
	Chimp	AAGTAATATT AGTAAGT TCACTGT	CTTTTCCTTATCC CAGAC CTTG
Large Mammals	Gorilla	AAGTAATATT AGTAAGT TCACTGT	CTTTTCCTTATCC CAGAC CTTG
	Cat	GAGTAGCATT AGCAGG CTTATTGT	CTTCCCCTTCTC CAGAC CTTA
	Dog	ACGTAATTTT AGCAGG CTTATTGT	CTTTGCCCTTATCC CAGAC CTTG
	Panda	GAGTAACATT AGCAGG CTTATTGT	CTTTCCCTTATCC CAGAC CTTG
	Cow	AAGTCATGTT AGCAGG CTTATTGC	CTTTCCCTAATGC CAGAT ATTG
	Bison	AAGTCATGTT AGTAGG CTTATTGC	CTTTCCCTAATGC CAGAT ATTG
	Sheep	AAGAAATGTT AGCAGG CTTATTGC	CTTTCCCTTATGC CAGAT ATTG
	Pig	AGGTAACATT AGCAGG CTCCTGC	CTTCCCCTTTT CAGAT CTTG
	Alpaca	AGGCAACATC AGCAGG CTCATTGT	TTTCCCCTTATCC CAGAT CTTG
	Horse	AAGTAACATT AGCAGG CTCATTGC	TTTCCCCTTATCC CAGAC CTCG
	Rhinoceros	AAGTAACGTT AGCAG ACTCATTGC	TTTTTCCTTATCC CAGAC CTCA
Bats	Armadillo	AGTTAACAT AGTAG ACACATTGG	-----
	Brown Bat	AAGT---GAC AGCAG CTCATTGA	CTTTTCCTTATT CAGAC TTTG
Rodents	Vampire Bat	AGGTAACATT AGCAGG CCCCGTTGC	CTTTCCCCTTATT CAGAC CTCG
	Rat	----AACCTT AGTAAG ATCACCAA	CTCTTCCTCATCC CAGAC CTCA
	Mouse	CC-----TT AGTAA ATCATCAA	CTCTTCCTCATCC CAGAT CTCA
	Marmot	AAGTAACATT AGTAGG CTCATAGC	GCTTTCCTTATCC CAGAC CTCG
	Squirrel	AAGTAACGTT AGTAGG CTCATAGC	CCTTTCCTTATCC CAGAC CTCG
	Hamster	AAAAAACCTT AGTGGG ATCACTGG	CTCTT----- CCAGAT CTCG
	Vole	AGGAAACCTT AGTGGG ATTGCCAG	CTCTTCTCCATCC CAGAT CTCA
Miscellaneous	Rabbit	AAGGAACATC AGTAGG CTCATGGT	CTGTTGTTTATCC CAGAC CTTA
	Hedgehog	AAGAATCAT AGTAG ACTGACTGC	CTTTACCTTTACC CAGAT CTGG
	Ferret	AAGTAACATT AGCAGG TTTACTGT	TTTCCCTCTCATCC CAGAC ATTG
	Shrew	GAGTGACAGC AGCAAG TTTCATGAC	TGTTCCCTTCTCCT GACCG TG
	Otter	AAGTAACATT AGCAGG TTTACTGT	CTTCCCCTCATCC CAGAC ATTG
	Seal	AAGTAACATT AGCAGG CTTATTGT	CTTTCCCTTATCC CAGAC CTAG
	Whale	AGGTAACATT AGCAGG CTTATTGC	CTTTCCCTTATGC CAGAT CTTG
	Dolphin	AGGTAACATT AGCAGG CTTATTGC	CTTTCCCTTATGC CAGAT CTTG

*

FIGURE 5 Multi-sequence alignment shows general conservation of ET splice sites across mammalian lineages. Multi-sequence alignment using Clustal Omega of the *F5* cDNA sequence around the 5' East Texas bleeding disorder (ET) donor splice site (shown is c.2340–2363) and the 3' ET acceptor splice site (shown is c.4442–4462), according to NM_000130.4, along with the corresponding sequences from other mammalian species. Residues at the ET splice junctions are in bold. The site of the missense variant in ET (c.A2350A>G) is marked with a star (*). Splice site consensus sequences for the major class of introns (U2 introns) generally consist of MAG/GTRAGT for the 5' splice site (where M is an A or C and R is an A or G) and CAG/G for the 3' splice sites.⁶⁹ The most common variant of non-consensus splice sites consists of a 5' splice site with a GC (blue text) instead of a GT; these GCAG introns have been purported to have enhanced matching at the 3' AG site.⁷⁰ Multi-sequence analysis of the ET splice sites confirms that the weak 5' ET site contains either a GT or GC and that the 3' splice site contains an AG in several mammalian species. FV, coagulation factor V

ET-spliced *F5* amplicon was seen using cells incorporating the *F5-ET* and *F5-ATL* transgenes (Figure 4A). Using the FLP-INTM 293 HEK cells (Figure 4B) a similar pattern was observed. In both cell types, an additional amplicon was present in the wt-*FL-F5* and *F5-ET* clones. Sanger sequencing of this amplicon revealed the same alternatively spliced transcript uncovered by RT-PCR using control human liver RNA (Figure 2E). This alternative splicing event predicts the in-frame removal of 1656 bp from exon 13, removing the FV BR but retaining AR2. Thus, this transcript could theoretically be translated into a viable FV-short-like protein although its physiologic relevance remains unknown. The contiguous sequence derived from Sanger sequencing this amplicon is included in Figure S1 in supporting information. Despite the benign prediction, it is possible one or more of the *F5* G-allele polymorphisms present in the wt-*FL-F5* cDNA contributed to splicing dysregulation and the production of this transcript. Overall, these data demonstrate the ability of heterologous mammalian cells to recapitulate ET-like splicing of *F5-ET*

and *F5-ATL* cDNA independent of *F5* introns and *F5* chromosomal context. Furthermore, these findings suggest that the machinery required for regulating *F5-short* splicing are present in other mammalian species (e.g., Syrian hamster) and non-hepatic cell types (e.g., kidney epithelium).

Multi-sequence alignment of the ET-splice sites showed general conservation across mammalian lineages (Figure 5). The increased ET-splicing driven by *F5-ATL* suggests that encoded within the *F5* cDNA at the region of *F5-ATL* are cis-acting regulatory elements responsible for controlling the use of the ET-splice sites. Based upon the upregulation of ET splicing with the removal of this region, we suspect this element represents an exonic splicing silencer sequence. *In silico* analysis using Human Splicing Finder 3.1⁴⁶ was performed on the 832 bp sequence deleted in *F5-ATL*. Several potential cis-acting splicing regulatory elements were predicted within this region including more than 250 silencer sequences (Table S6 in supporting information).

4 | DISCUSSION

Factor V is a multifaceted protein with clear roles in regulating blood coagulation. Exon 13 of *F5* is large, highly repetitive, poorly conserved, and encodes the entire B-domain, a domain not necessary for procoagulant function. However, the B-domain contains a bipartite autoinhibitory domain (the BR and AR2) crucial for maintaining an inactive procofactor state. Missense variants in *F5* exon 13 have been identified in patients with bleeding diatheses and have brought to light a novel regulatory function: the FV cofactor function in the TFPI anticoagulant pathway.^{11,13,47} Herein, we describe a novel sequence variant in *F5* exon 13 and demonstrate unexpected yet markedly enhanced ET-splicing originating from the variant allele. Although *F5-ATL* shares a commonality with ET and FV-Amsterdam in the enhanced production of FV-short and elevated TFPI levels, the molecular genetics are different, and the phenotypic effect appears greater. Enhanced ET splicing directly associated with the *F5-ATL* allele suggests the presence of previously unrecognized regulatory elements encoded within *F5* exon 13. Alterations in this region of *F5* may be distinctly involved in modulating the TFPI anticoagulant pathway. This work implies that any formerly ascribed benign polymorphisms within this region may in fact have functional significance. It also suggests the presence of a novel axis for controlling hemostatic balance.

F5-ATL was identified in a patient with severe bleeding. Definitively proving the clinical causality of *F5-ATL* on this patient's bleeding is beyond the scope of this study, especially as additional family members and further patient samples are not available. Yet, the collective data presented herein support its pathogenicity. Analysis of patient cDNA using RT-PCR, RNAseq, and Sanger sequencing identified enhanced ET-splicing originating exclusively from the variant allele. Biochemical studies using patient plasma revealed increased TFPI and FV-short at levels previously undescribed. In *F5-ATL* patient plasma, FL-FV was present at approximately one-half the concentration of FL-FV in NHP. This concentration is expected based on the presence of one fully functional *F5* allele, and this implies that at least ~50% of this patient's FV should function normally. RNAseq results suggest that in this patient FV-short levels should approximate FL-FV levels. Yet, FV-short was substantially elevated (~45 nM), raising the total FV plasma concentration well above that seen in NHP. One key limitation of this result is the lack of an available validated assay to quantitatively measure FV-short, especially in the presence of significant TFPI elevations. The results presented are semi-quantitative and suggest significantly elevated levels of FV-short. The increase in FV-short seen in patient plasma may result from enhanced expression, increased mRNA stability, and/or improved protein secretion. Enhanced stabilization of FV-short in plasma afforded by TFPI α binding may also be contributory. Recently published *in vitro* studies confirm the constitutive activity of FV-short but also demonstrate that binding of the TFPI α basic region to FV-short AR2 delays thrombin cleavage at Arg-1545.^{30,48} However, once activated by thrombin, TFPI α has no effect on FVa function. Despite this, the addition of FV-short to NHP appears to

decrease peak thrombin; the mechanism of this decrease remains unknown.⁴⁷ The precise effects of FV-short and the FV-short/TFPI interaction on global hemostatic balance *in vivo* remains to be determined. Further studies delineating the role of FV-short in hemostasis may shed light on the pathophysiology associated with such remarkable elevations in FV-short as seen in this patient. In addition to FV-short, both total and free TFPI were significantly increased. As TFPI α is the only isoform capable of interacting with FV-short, this was not anticipated. Measurement of TFPI levels is also limited by the lack of a validated quantitative assay, and competition between anti-TFPI antibodies and FV-short may confound these results. In plasma, TFPI consists of full-length and C-terminally truncated variants.^{14,49} We speculate the increase in total TFPI originates from accumulation of C-terminally truncated isoforms derived from increased TFPI α . We surmise that the high TFPI levels and resultant anticoagulant effects along with potential alterations in FV-short function contribute to this patient's bleeding. The potential role of TFPI in this patient's bleeding is supported by the normalization of the lag time and peak thrombin on TGA with the addition of TFPI blockade. The bleeding phenotype associated with ET and FV-Amsterdam, which is speculated to result from elevated plasma TFPI, and the bleeding events seen in the clinical trials investigating both recombinant TFPI α in sepsis and BAX499, an anti-TFPI aptamer that unexpectedly elevated plasma full-length TFPI add plausibility regarding the influence of TFPI on the *F5-ATL* patient's bleeding.^{50,51}

Alternative splicing is a powerful mediator of transcriptome diversity. By selectively including or excluding segments of pre-mRNA, alternative splicing can dramatically alter the cellular protein repertoire. Recent studies suggest the variety of alternatively spliced transcripts is much greater than previously appreciated^{52,53} and that splicing should be viewed as a competitive process whereby splicing machinery must discriminate among numerous splice sites. Splicing is highly tissue dependent. Hepatocytes are the physiologic site of FV biosynthesis in humans; due to accessibility, ectopic transcripts derived from leukocytes were utilized in this study. Thus, interpretation of these results is limited by the lack of liver-specific structural changes and post-transcriptional processing. In the *F5-ATL* patient samples, the predominant *F5* transcripts correspond to FL-*F5* and ET-spliced *F5*. However, using RT-PCR, additional *F5* exon 13 alternatively spliced isoforms were identified. These transcripts include *F5* transcripts predicted to produce a FV-short-like protein yet utilizing alternative cryptic splice sites and *F5* transcripts skipping exon 13 entirely. RNAseq on our control samples failed to identify these transcripts and ET-spliced *F5* transcripts. However, detection of low-abundance transcripts is notoriously difficult, and PCR-based methods are more sensitive for identifying low-frequency transcripts in comparison to RNAseq.^{45,54} Furthermore, the highly repetitive nature of *F5* exon 13 as well as the short read lengths intrinsic to traditional next-generation sequencing are limitations of assessing the *F5* transcriptome using this technique. In the *F5-ATL* patient samples, transcripts containing the 832 bp deletion were only identified on RT-PCR using primers directly flanking the deletion (with one

primer residing within the ET-spliced region) and were not seen via RNAseq. This implies that any canonically spliced transcript containing this deletion undergoes nonsense-mediated decay, as would be predicted by the terminal frameshift. In contrast, in our heterologous cell model incorporating *F5-ATL* cDNA, the predominant species represents a canonically spliced transcript containing *F5-ATL*, which should undergo nonsense-mediated decay. However, as mRNA splicing is a prerequisite for nonsense-mediated decay, this quality control mechanism is likely not operational in this system.⁵⁵

In the classical view, splicing is regulated by cis-acting sequence motifs and trans-acting factors that bind these elements. RNAseq using the *F5-ATL* patient's leukocytes revealed that ET-spliced transcripts represent ~50% of the total *F5* mRNA pool, and mapping of these ET-spliced transcripts demonstrated that they originate from the *F5-ATL* allele. This finding suggests that encoded in *F5* at the region of *F5-ATL* is a cis-acting regulatory element capable of suppressing splicing at the ET splice sites. Removal of this element through genetic deletion would facilitate upregulation of ET splicing and the production of higher levels of *F5-short* mRNA. Heterologous expression of *F5-ATL* in mammalian cells confirmed increased relative expression of *F5-short* transcripts compared to that achieved using a wt-*FL-F5* and *F5-ET* transgenes. However, in these cells, splicing at the ET-splice sites is not as efficient as within the *F5-ATL* patient. This likely relates to features of the artificial cell culture model including the marked overexpression of *F5*-variant cDNA, promoter-mediated effects on transcription kinetics and transcription activators,⁵⁶ and the lack of *F5* introns.^{55,57} Overall, the data support the notion that evolutionarily conserved signals are responsible for controlling *F5-short* splicing and suggest that splicing regulatory elements 3' to the ET donor site play a major role in driving alternative splicing in this region. To date, only a limited number of splicing regulatory elements have been described, and due to their often degenerate nature, identification and functional characterization remain challenging.⁵⁸⁻⁶⁰ Nonetheless, to discover potential cis-acting elements, *in silico* analysis of the region of *F5* deleted in *F5-ATL* was undertaken and yielded numerous potential regulatory sequences spread throughout the *F5-ATL* deleted region. Ongoing studies seek to define the splicing regulatory elements and mechanism(s) involved in *F5-short* splicing.

Alternative splicing is capable of context-dependent dynamic regulation⁶¹ and has been shown to (1) drive maturation and differentiation of numerous tissues,^{62,63} (2) enhance neuronal plasticity,⁶⁴ and (3) augment immune responses.^{65,66} Up to 60% of human disease-causing variants have been estimated to disrupt splicing, and a significant proportion of population-based benign variants may impact splicing.^{67,68} We propose that alternative splicing represents a regulatory component involved in dynamically controlling hemostasis. Deciphering the regulatory elements involved in *F5* splicing may incite new avenues of research exploring alternative splicing as a mediator of context-dependent hemostatic regulation. Furthermore, advances in our understanding of the intricate and tightly regulated mechanisms involved in maintaining hemostatic

balance may uncover novel pharmaceutical targets to improve the management of patients with bleeding diatheses and pathogenic thromboses.

ACKNOWLEDGMENTS

This work was supported by funding from the National Institutes of Health/National Heart, Lung and Blood Institute (R56-HL131059 and R01-137128 to C.B.D. and R01-HL131833 and P01-HL139420 to R.M.C.). R.M.C. also receives research funding from Pfizer and Bayer. Additionally, this study was supported in part by funding from the NHF-Shire Clinical Fellowship Program and from the Pfizer Global ASPIRE Gene and anti-TFPI Therapies Hemophilia Program (WI242430 to K.L.Z.). This study was supported in part by the Emory Integrated Genomics Core (EIGC), which is subsidized by the Emory University School of Medicine and is one of the Emory Integrated Core Facilities.

CONFLICTS OF INTEREST

R.M. Camire is a consultant for and receives research support from Pfizer and Bayer. K.L. Zimowski receives research support from Pfizer. C.L. Kempton has received honoraria for participation in medical advisory boards from Spark Therapeutics and Octapharma and research support from Novo Nordisk. C.B. Doering is a cofounder of Expression Therapeutics and owns equity in this company. The remaining authors (T. Petrillo, M.D. Ho, J. Wechsler, J.E. Shields, G. Denning, N. Jhita, A.A. Rivera, and M.A. Escobar) have no relevant conflicts of interest to disclose.

AUTHOR CONTRIBUTIONS

C.B. Doering, C.L. Kempton, and R.M. Camire conceived the study. K.L. Zimowski, M.D. Ho, T. Petrillo, A.A. Rivera, J.E. Shields, N. Jhita, G. Denning, J. Wechsler, M. Escobar, and C.L. Kempton conducted the experiments. K.L. Zimowski, T. Petrillo, C.B. Doering, and R.M. Camire analyzed the data and wrote the manuscript. All authors reviewed this manuscript prior to submission.

ORCID

Karen L. Zimowski  <https://orcid.org/0000-0003-3819-7200>

REFERENCES

1. Cripe LD, Moore KD, Kane WH. Structure of the gene for human coagulation factor V. *Biochemistry*. 1992;31:3777-3785.
2. Jenny RJ, Pittman DD, Toole JJ, et al. Complete cDNA and derived amino acid sequence of human factor V. *Proc Natl Acad Sci USA*. 1987;84:4846-4850.
3. Kane WH, Davie EW. Cloning of a cDNA coding for human factor V, a blood coagulation factor homologous to factor VIII and ceruloplasmin. *Proc Natl Acad Sci USA*. 1986;83:6800-6804.
4. Kane WH, Ichinose A, Hagen FS, Davie EW. Cloning of cDNAs coding for the heavy chain region and connecting region of human factor V, a blood coagulation factor with four types of internal repeats. *Biochemistry*. 1987;26:6508-6514.
5. Monkovic DD, Tracy PB. Activation of human factor V by factor Xa and thrombin. *Biochemistry*. 1990;29:1118-1128.
6. Camire RM, Bos MHA. The molecular basis of factor V and VIII procofactor activation. *J Thromb Haemost*. 2009;7:1951-1961.

7. Bos MHA, Camire RM. A Bipartite autoinhibitory region within the B-domain suppresses function in factor V. *J Biol Chem*. 2012;287:26342-26351.
8. Bunce MW, Bos MHA, Krishnaswamy S, Camire RM. Restoring the procofactor state of factor Va-like variants by complementation with B-domain peptides. *J Biol Chem*. 2013;288:30151-30160.
9. Toso R, Camire RM. Removal of B-domain sequences from factor V rather than specific proteolysis underlies the mechanism by which cofactor function is realized. *J Biol Chem*. 2004;279:21643-21650.
10. Zhu H, Toso R, Camire RM. Inhibitory sequences within the B-domain stabilize circulating factor V in an inactive state. *J Biol Chem*. 2007;282:15033-15039.
11. Cunha ML, Bakhtiari K, Peter J, Marquart JA, Meijers JC, Middeldorp S. A novel mutation in the F5 gene (factor V Amsterdam) associated with bleeding independent of factor V procoagulant function. *Blood*. 2015;125:1822-1825.
12. Kuang SQ, Hasham S, Phillips MD, et al. Characterization of a novel autosomal dominant bleeding disorder in a large kindred from east Texas. *Blood*. 2001;97:1549-1554.
13. Vincent LM, Tran S, Livaja R, Bensend TA, Milewicz DM, Dahlbäck B. Coagulation factor VA2440G causes east Texas bleeding disorder via TFPI α . *J Clin Invest*. 2013;123:3777-3787.
14. Broze GJ, Girard TJ. Tissue factor pathway inhibitor: structure-function. *Front Biosci*. 2012;17:262-280.
15. Mast AE. Tissue factor pathway inhibitor. *Arterioscler Thromb Vasc Biol*. 2016;36(1):9-14.
16. Maroney SA, Mast AE. New insights into the biology of tissue factor pathway inhibitor. *J Thromb Haemost*. 2015;13.
17. Wood JP, Ellery PER, Maroney SA, Mast AE. Biology of tissue factor pathway inhibitor. *Blood*. 2014;123:2934-2943.
18. Ndonwi M, Girard TJ, Broze GJ. The C-terminus of tissue factor pathway inhibitor α is required for its interaction with factors V and Va. *J Thromb Haemost*. 2012;10:1944-1946.
19. Duckers C, Simioni P, Rosing J, Castoldi E. Advances in understanding the bleeding diathesis in factor V deficiency. *Br J Haematol*. 2009;146:17-26.
20. Wood JP, Bunce MW, Maroney SA, Tracy PB, Camire RM, Mast AE. Tissue factor pathway inhibitor-alpha inhibits prothrombinase during the initiation of blood coagulation. *Proc Natl Acad Sci USA*. 2013;110:17838-17843.
21. Girard TJ, Warren LA, Novotny WF, et al. Functional significance of the Kunitz-type inhibitory domains of lipoprotein-associated coagulation inhibitor. *Nature*. 1989;338:518-520.
22. Hackeng TM, Seré KM, Tans G, Rosing J. Protein S stimulates inhibition of the tissue factor pathway by tissue factor pathway inhibitor. *Proc Natl Acad Sci USA*. 2006;103:3106-3111.
23. Ndonwi M, Tuley EA, Broze GJ. The Kunitz-3 domain of TFPI- α is required for protein S-dependent enhancement of factor Xa inhibition. *Blood*. 2010;116:1344-1351.
24. Mast AE, Broze GJ. Physiological concentrations of tissue factor pathway inhibitor do not inhibit prothrombinase. *Blood*. 1996;87:1845-1850.
25. Duckers C, Simioni P, Spiezia L, et al. Low plasma levels of tissue factor pathway inhibitor in patients with congenital factor V deficiency. *Blood*. 2008;112:3615-3623.
26. Shao Y, Wu W, Xu G, Wang X, Ding Q. Low factor V level ameliorates bleeding diathesis in patients with combined deficiency of factor V and factor VIII. *Blood*. 2019;134:1745-1754.
27. van Doorn P, Rosing J, Duckers C, Hackeng TM, Simioni P, Castoldi E. Factor V has anticoagulant activity in plasma in the presence of TFPI α : difference between FV1 and FV2. *Thromb Haemost*. 2018;118:1194-1202.
28. Dahlbäck B. Novel insights into the regulation of coagulation by factor V isoforms, tissue factor pathway inhibitor α , and protein S. *J Thromb Haemost*. 2017;15:1241-1250.
29. Peraramelli S, Thomassen S, Heinzmann A, et al. Role of exosite binding modulators in the inhibition of Fxa by TFPI. *Thromb Haemost*. 2016;115:580-590.
30. van Doorn P, Rosing J, Wielders SJ, Hackeng TM, Castoldi E. The C-terminus of tissue factor pathway inhibitor- α inhibits factor V activation by protecting the Arg1545 cleavage site. *J Thromb Haemost*. 2017;15:140-149.
31. Bunce MW, Toso R, Camire RM. Zymogen-like factor Xa variants restore thrombin generation and effectively bypass the intrinsic pathway in vitro. *Blood*. 2011;117:290-298.
32. Varadi K, Siekmann J, Turecek PL, Schwarz HP, Marder VJ. Phospholipid-bound tissue factor modulates both thrombin generation and APC-mediated factor Va inactivation. *Thromb Haemost*. 1999;82:1673-1679.
33. Andrews S. FastQC: A quality control tool for high throughput sequence data 2010. Available from: <http://www.bioinformatics.babraham.ac.uk/projects/fastqc/>
34. Dobin A, Davis CA, Schlesinger F, et al. STAR: ultrafast universal RNA-seq aligner. *Bioinformatics*. 2012;29:15-21.
35. Li H, Handsaker B, Wysoker A, et al. The sequence alignment/map format and SAMtools. *Bioinformatics*. 2009;25:2078-2079.
36. PicardTools. Available from: <http://broadinstitute.github.io/picard/>
37. Robinson JT, Thorvaldsdóttir H, Winckler W, et al. Integrative genomics viewer. *Nat Biotechnol*. 2011;29:24-26.
38. Kostka H, Schwarz T, Schellong S, et al. Coagulation factor V G allele and HR2 haplotype: factor V activity, activated protein C resistance and risk of venous thrombosis. *Blood Coagul Fibrinolysis*. 2003;14:49-56.
39. Tracy PB, Eide LL, Bowie EJ, Mann KG. Radioimmunoassay of factor V in human plasma and platelets. *Blood*. 1982;60:59-63.
40. Bloemen S, Huskens D, Konings J, et al. Interindividual variability and normal ranges of whole blood and plasma thrombin generation. *J Appl Lab Med*. 2017;2:150-164.
41. Dargaud Y, Luddington R, Gray E, et al. Standardisation of thrombin generation test - which reference plasma for TGT? An international multicentre study. *Thromb Res*. 2010;125:353-356.
42. Gerotziafas GT, Depasse F, Busson J, Leflem L, Elalamy I, Samama MM. Towards a standardization of thrombin generation assessment: The influence of tissue factor, platelets and phospholipids concentration on the normal values of Thrombogram-Thrombinoscope assay. *Thromb J*. 2005;3:16.
43. Viel KR, Ameri A, Abshire TC, et al. Inhibitors of factor VIII in black patients with hemophilia. *N Engl J Med*. 2009;360:1618-1627.
44. Halvardson J, Zaghlool A, Feuk L. Exome RNA sequencing reveals rare and novel alternative transcripts. *Nucleic Acids Res*. 2013;41(1):e6.
45. Mehta S, Tsai P, Lasham A, et al. A study of TP53 RNA splicing illustrates pitfalls of RNA-seq methodology. *Can Res*. 2016;76:7151-7159.
46. Desmet F-O, Hamroun D, Lalande M, Collod-Bérout G, Claustres M, Bérout C. Human Splicing Finder: an online bioinformatics tool to predict splicing signals. *Nucleic Acids Res*. 2009;37.
47. Dahlbäck B, Guo L, Livaja-Koshir R, Tran S. Factor V-short and protein S as synergistic tissue factor pathway inhibitor (TFPI α) cofactors. *Res Pract Thromb Haemost*. 2018;2:114-124.
48. Petrillo T, Ayombil F, Veer C, Camire RM. Regulation of factor V and factor V-short by TFPI α : Relationship between B-domain proteolysis and binding. *J Biol Chem*. 2021;296:100234.
49. Abumiya T, Enjoji K, Kokawa T, Kamikubo Y, Kato H. An anti-tissue factor pathway inhibitor (TFPI) monoclonal antibody recognized the third Kunitz domain (K3) of free-form TFPI but not lipoprotein-associated forms in plasma. *J Biochem*. 1995;118:178-182.
50. Dockal M, Pachlinger R, Hartmann R, et al. biological explanation of clinically observed elevation of TFPI plasma levels after treatment with TFPI-antagonistic aptamer BAX 499. *Blood*. 2012;120(21):1104.

51. Abraham E, Reinhart K, Opal S, et al. Efficacy and safety of tifa-cogin (recombinant tissue factor pathway inhibitor) in severe sepsis: a randomized controlled trial. *JAMA*. 2003;290:238-247.
52. Dvinge H. Regulation of alternative mRNA splicing: old players and new perspectives. *FEBS Lett*. 2018;592:2987-3006.
53. Lee Y, Rio DC. Mechanisms and regulation of alternative pre-mRNA splicing. *Annu Rev Biochem*. 2015;84:291-323.
54. Wang F, Zhao Y, Hao Y, Tan Z. Identification of low-abundance alternatively spliced mRNA variants by exon exclusive reverse transcriptase polymerase chain reaction. *Anal Biochem*. 2008;383:307-310.
55. Kurosaki T, Popp MW, Maquat LE. Quality and quantity control of gene expression by nonsense-mediated mRNA decay. *Nat Rev Mol Cell Biol*. 2019;20:406-420.
56. Nogués G, Kadener S, Cramer P, Bentley D, Kornblihtt AR. Transcriptional activators differ in their abilities to control alternative splicing. *J Biol Chem*. 2002;277:43110-43114.
57. Zhang J, Sun X, Qian Y, LaDuca JP, Maquat LE. At least one intron is required for the nonsense-mediated decay of triosephosphate isomerase mRNA: a possible link between nuclear splicing and cytoplasmic translation. *Mol Cell Biol*. 1998;18:5272-5283.
58. Wang Z, Xiao X, Van Nostrand E, Burge CB. General and specific functions of exonic splicing silencers in splicing control. *Mol Cell*. 2006;23:61-70.
59. Wang Z, Rolish ME, Yeo G, Tung V, Mawson M, Burge CB. Systematic identification and analysis of exonic splicing silencers. *Cell*. 2004;119:831-845.
60. Goren A, Ram O, Amit M, et al. Comparative analysis identifies exonic splicing regulatory sequences—the complex definition of enhancers and silencers. *Mol Cell*. 2006;22:769-781.
61. Baralle FE, Giudice J. Alternative splicing as a regulator of development and tissue identity. *Nat Rev Mol Cell Biol*. 2017;18:437-451.
62. Pimentel H, Parra M, Gee S, et al. A dynamic alternative splicing program regulates gene expression during terminal erythropoiesis. *Nucleic Acids Res*. 2014;42:4031-4042.
63. Wong J, Ritchie W, Ebner OA, et al. Orchestrated intron retention regulates normal granulocyte differentiation. *Cell*. 2013;154:583-595.
64. Furlanis E, Scheffele P. Regulation of neuronal differentiation, function, and plasticity by alternative splicing. *Annu Rev Cell Dev Biol*. 2018;34:1-19.
65. Martinez NM, Lynch KW. Control of alternative splicing in immune responses: many regulators, many predictions, much still to learn. *Immunol Rev*. 2013;253:216-236.
66. Rodrigues R, Grosso A, Moita L. Genome-wide analysis of alternative splicing during dendritic cell response to a bacterial challenge. *PLoS ONE*. 2013;8(4):e61975.
67. Wang G-S, Cooper TA. Splicing in disease: disruption of the splicing code and the decoding machinery. *Nat Rev Genet*. 2007;8(10):749-761.
68. Li YI, van de Geijn B, Raj A, et al. RNA splicing is a primary link between genetic variation and disease. *Science*. 2016;352:600-604.
69. Zhang MQ. Statistical features of human exons and their flanking regions. *Hum Mol Genet*. 1998;7:919-932.
70. Thanaraj TA, Clark F. Human GC-AG alternative intron isoforms with weak donor sites show enhanced consensus at acceptor exon positions. *Nucleic Acids Res*. 2001;29:2581-2593.

SUPPORTING INFORMATION

Additional supporting information may be found online in the Supporting Information section.

How to cite this article: Zimowski KL, Petrillo T, Ho MD, et al. *F5-Atlanta*: A novel mutation in *F5* associated with enhanced East Texas splicing and FV-short production. *J Thromb Haemost*. 2021;19:1653-1665. <https://doi.org/10.1111/jth.15314>